Ring-Opening and Meso Substitution from the Reaction of Cyanide Ion with Zinc Verdohemes

James A. Johnson, Marilyn M. Olmstead, Alan M. Stolzenberg,† and Alan L. Balch*

Department of Chemistry, University of California, Davis, California 95616

Received March 26, 2001

The reactivity of zinc verdoheme, $[Zn^{II}(OEOP)](O_2CCH_3)$ where OEOP is the monoanion of octaethyl-5-oxaporphyrin, with cyanide ion has been shown to be a complex process that involves not only the expected ring-opening of the macrocycle, as occurs with other nucleophiles (methoxide, methanethiolate, dimethylamide), but also substitution at one or two of the meso positions. The ring-opened products have been subjected to crystallographic study. The structures of μ-H_2O-$\{Zn^{II}(OEB\text{-}10,19\text{-}(CN)_2)\}_2$ and μ-H_2O-$\{(Zn^{II}(OEB\text{-}10,15,19\text{-}(CN)_3)\}_2$ both consist of two helical tetrapyrrole subunits that are coordinated to a zinc ion through four Zn−N bonds. The two zinc ions are coordinated to a bridging water molecule that is also hydrogen bonded to a lactam oxygen atom at one end of each tetrapyrrole subunit. Thus the chiral sense of one helical $Zn^{II}(OEB\text{-}10,19\text{-}(CN)_2)$ portion is transmitted to the other $Zn^{II}(OEB\text{-}10,19\text{-}(CN)_2)$ unit and the resulting binuclear unit is chiral. In contrast $Co^{II}(OEB\text{-}15,19\text{-}(CN)_2)$, which was obtained by the insertion of Co(II) into the free ligand, is monomeric with a four-coordinate cobalt ion. A series of DFT geometry optimization calculations were performed on zinc complexes of 5-oxaporphyrins (verdoheme), verdins (bilindione), 4-cyano-5-oxaporphyrins, and 19-cyanoverdins in an effort to gain insights to the features of these complexes and the reactions that lead to *meso*-cyano-substituted cyanoverdins.

Introduction

As seen in Scheme 1, the 5-oxaporphyrin macrocycle can be synthesized from porphyrins by the process of coupled oxidation[1,2] or by the dehydration of biliverdin in the presence of a metal ion.[3] Scheme 2 shows the numbering scheme used for the various tetrapyrroles discussed in this article. In the process of coupled oxidation an iron or cobalt porphyrin is oxidized by molecular oxygen in the presence of a strongly coordinating ligand (pyridine or cyanide ion) and a reducing agent (ascorbic acid or hydrazine).[2,4−6] Metal complexes of the 5-oxaporphyrin macrocycle are generally deep green in color and are known as verdohemes.[7,8,9] The 5-oxaporphyrin macrocycle is also produced as a detectable intermediate in heme cleavage caused by the enzyme heme oxygenase.[10]

Although the 5-oxaporphyrin macrocycle resembles the corresponding porphyrin in structure, it is much more vulnerable to attack by anionic nucleophiles. Previous work from this laboratory has conclusively shown that treatment of iron(II), cobalt(II), and zinc(II) verdoheme complexes of the 5-oxaoctaethylporphyrins, $[Fe^{II}(OEOP)]^+$, $[Co^{II}(OEOP)]^+$, and $[Zn^{II}(OEOP)]^+$, with methoxide ion results in ring-opening to produce metal complexes that contain the dianion of the open-chain tetrapyrrole, $[OEBOMe]^-$, as seen in Scheme 3.[11,12] Additional work from this laboratory has shown that $[Zn^{II}(OEOP)]^+$ reacts with thiolate and amide ions to produce the helical, open-chain tetrapyrrole complexes, $Zn^{II}(OEBSMe)$ and $Zn^{II}(OEBNMe_2)$, as again seen in Scheme 3.[13] Presumably, these ring-opening reactions proceed through nucleophilic attack on one of the carbon atoms adjacent to the oxygen atom of the verdoheme to form initially a tetrahedral carbon atom which subsequently opens to form the verdoheme structure.

In this article we examine the reactions of cyanide ion with the 5-oxaporphyrin ligand. During studies of the coupled oxidation of $Fe^{III}(OEP)Cl$ in the presence of cyanide ion,[6] we found that the process was highly dependent on the specific reaction conditions, in particular the efficiency of mass transport of air into the reaction mixture and the duration of the reaction. When $Fe^{II}(OEP)$ is oxidized under coupled oxidation conditions in the presence of cyanide ion but with stirring that is not sufficiently rapid to produce turbulence,[6] the yield of the verdoheme $\{(NC)_2Fe(OEOP)\}$ is reduced and at least 10 new products form. One of these, $H_2(OEB\text{-}15,19\text{-}(CN)_2)$, is a ring-opened tetrapyrrole that contains two, rather than the expected one, added cyanide substituents. In order to completely characterize this material and to explore the reactions that led to its existence, a study of the reactivity of verdohemes with cyanide

† Permanent address: Department of Chemistry, PO Box 6045, West Virginia University, Morgantown, WV 26506-6045.

(1) Warburg, O.; Negelein, E. *Chem. Ber.* **1930**, *63*, 1816.
(2) St. Claire, T. N.; Balch, A. L. *Inorg. Chem.* **1999**, *38*, 684.
(3) Saito, S.; Itano, H. A. *J. Chem. Soc., Perkin Trans. 1* **1986**, 1.
(4) Balch, A. L.; Mazzanti, M.; Olmstead, M. M. *J. Chem. Soc., Chem. Commun.* **1994**, 269.
(5) Balch, A. L.; Mazzanti, M.; St. Claire, T. N.; Olmstead, M. M. *Inorg. Chem.* **1995**, *34*, 2194.
(6) Balch, A. L.; Koerner, R.; Latos-Grażyński, L.; Lewis, J. E.; St. Claire, T. N.; Zovinka, E. P. *Inorg. Chem.* **1997**, *36*, 3892.
(7) Lagarias, J. C. *Biochim. Biophys. Acta* **1982**, *717*, 12.
(8) Balch, A. L.; Latos-Grażyński, L.; Noll, B. C.; Olmstead, M. M.; Szerenberg, L.; Safari, N. *J. Am. Chem. Soc.* **1993**, *115*, 1422.
(9) Balch, A. L.; Koerner, R.; Olmstead, M. M. *J. Chem. Soc., Chem. Commun.* **1995**, 873.
(10) Liu, Y.; Moenne-Loccoz, P.; Loehr, T. M.; Ortiz de Montellano, P. R. *J. Biol. Chem.* **1997**, *272*, 6909.
(11) Koerner, R.; Latos-Grażyński, L.; Balch, A. L. *J. Am. Chem. Soc.* **1998**, *120*, 9246.
(12) Latos-Grażyński L.; Johnson, J.; Attar, S.; Olmstead, M. M.; Balch, A. L. *Inorg. Chem.* **1998**, *37*, 4493.
(13) Johnson, J. A.; Olmstead, M. M.; Balch, A. L. *Inorg. Chem.* **1999**, *38*, 5379.

10.1021/ic0103300 CCC: $20.00 © 2001 American Chemical Society
Published on Web 09/18/2001

Scheme 1

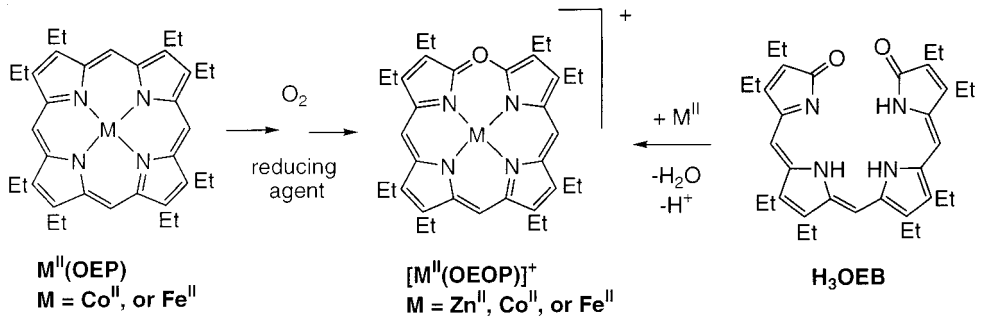

Scheme 2

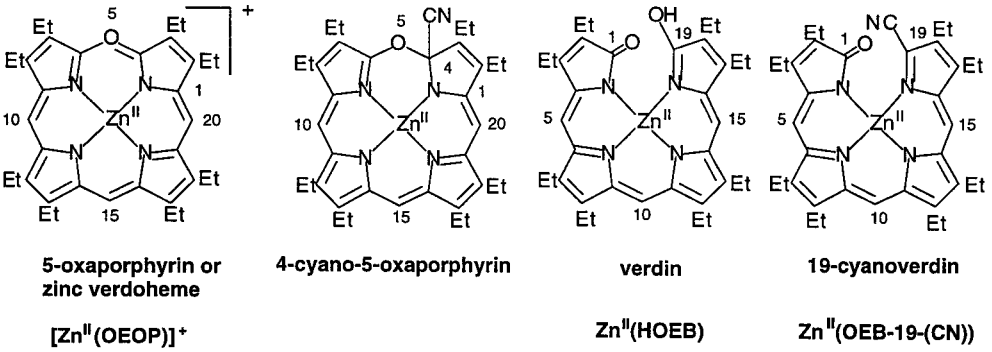

Scheme 3

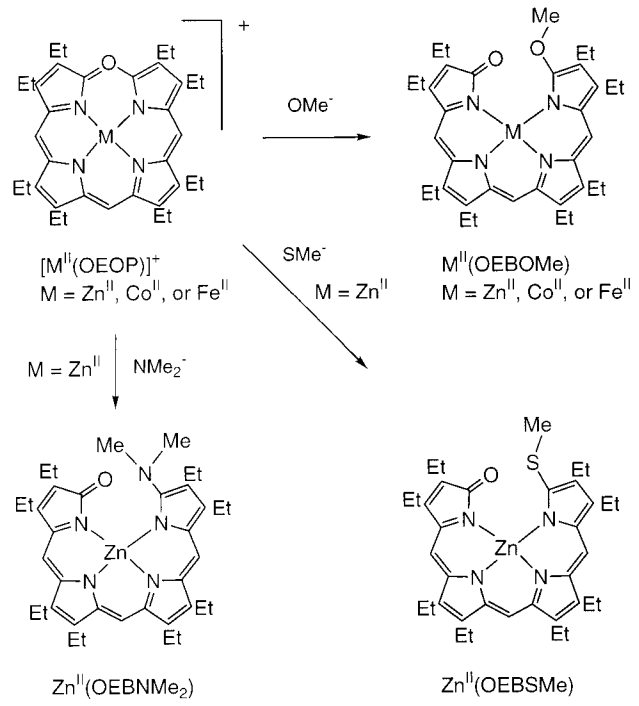

ion was undertaken. To facilitate isolation of stable products, the addition of cyanide ion to the zinc complex [Zn^{II}(OEOP)](O_2CCH_3) was examined. Previous work indicated that the zinc complexes of the open-chain tetrapyrroles are significantly more stable than their cobalt(II) and iron(II) analogues.[11−13] Moreover, the use of the zinc complexes minimized complications from metal-centered redox reactions.

Results

Isolation of H_2(OEB-15,19-$(CN)_2$) from the Coupled Oxidation of $ClFe^{III}$(OEP) with Cyanide and Ascorbate. Reaction of $ClFe^{III}$(OEP) with large excesses of potassium cyanide and ascorbic acid in methanol with rapid, but nonturbulent, stirring produces a muddy, brown-green solution. This contrasts with the previously reported translucent green solution that is obtained with turbulent stirring.[6] Workup of the reaction proceeds with some difficulty to afford a brown solid rather than the expected dark blue, crystalline solid {$(NC)_2Fe^{III}$(OEOP)}. Separation of the product mixture by preparative thin-layer chromatography results in 4 major and 6 minor resolved bands. One of the major bands contains the known compound octaethylbiliverdin, H_3(OEB). Another major band affords a yellow-green compound, which we identified as H_2(OEB-15,19-$(CN)_2$), below. The relative amounts of material contained in the different TLC bands varied with the duration of the reaction. The amount of H_2(OEB-15,19-$(CN)_2$) present increases when the reaction time is lengthened from 3 h to roughly 11 h, but decreases at extended times. The other products of this reaction remain unidentified at this time. Since such a complex mixture of products was obtained, we did not pursue this route as a means of preparing other cyanoverdins.

The UV/vis spectrum of H_2(OEB-15,19-$(CN)_2$) is shown in trace B of Figure 1. The spectrum has a broad absorption at 420 nm, a region typical of a porphyrin Soret band, and a lower intensity absorption at 778 nm. The number, shapes, and relative intensities of the spectral bands resemble those of octaethylformylbiliverdin, H_2(OEFB),[14,15] except that the visible bands are red-shifted by roughly 50 nm and the Soret band by 15 nm. The presence of two broad N−H resonances at 12.60 and 8.81 ppm in the ^{1}H NMR spectrum of the compound establishes that it is a free base rather than a metal complex. The ^{1}H NMR spectrum also resembles that of H_2(OEFB) but differs in the respect that a formyl proton peak is absent, only two rather than

(14) Wasser, P. K. W.; Fuhrhop, J.-H. *Ann. N.Y. Acad. Sci.* **1973**, *206*, 533.
(15) Koerner, R.; Olmstead, M. M.; Ozarowski, A.; Phillips, S. L.; Van Calcar, P. M.; Winkler, K.; Balch, A. L. *J. Am. Chem. Soc.* **1998**, *120*, 1274.

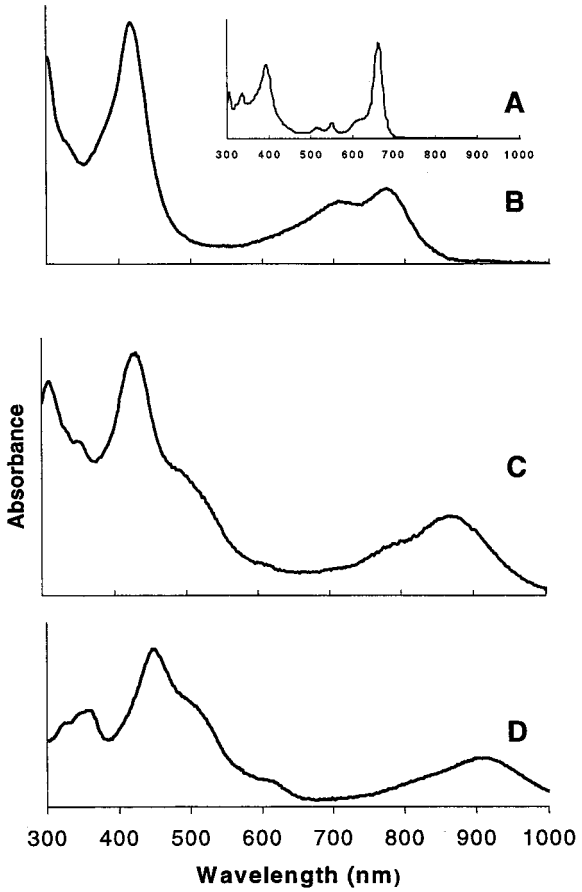

Figure 1. Inset A shows the UV/vis spectrum of blue-green [Zn^{II}(OEOP)](O_2CCH_3) for comparison. Electronic absorption spectra of (B) green H_2(OEB-15,19-$(CN)_2$) [λ_{max}, nm (ϵ, M^{-1} cm^{-1}) (relative absorbance): 302 (0.83), 412 (1.00), 722 sh (0.25), 778 (0.33)]; (C) brown Zn^{II}(OEB-15,19-$(CN)_2$) [λ_{max}, nm (ϵ, M^{-1} cm^{-1}): 308 (12000), 430 (16300), 796 (3800), 868 (5700)]; and (D) brown Zn^{II}(OEB-10,-15,19-$(CN)_3$) [λ_{max}, nm (ϵ, M^{-1} cm^{-1}): 444 (13700), 906 (3480)], all in chloroform.

three methine resonances are observed in the range 6−7 ppm, and the dispersion of the ethyl group CH_2 quartets and CH_3 triplets is greater than in OEFB. Insertion of zinc into H_2(OEB-15,19-$(CN)_2$) led to little change in the ^{1}H NMR spectrum other than loss of the N−H resonances at 12.60 and 8.81 ppm. However, zinc insertion results in a dramatic 90 nm red shift of the visible absorption spectral band to 871 nm.

The UV/vis and ^{1}H NMR data suggest that the yellow-green compound formally is derived from OEFB by replacement of the formyl group and one methine proton with cyano groups. This is confirmed by the MALDI mass spectrum of the compound, which shows a parent ion peak at *m*/*e* 611.3406 ($C_{37}H_{44}N_6O + Na^+$). The only dipyrrolic fragment observed has *m*/*e* 283.1792. This corresponds to a $C_{18}H_{23}N_2O$ fragment resulting from scission at the C10−C11 bond and is identical to the dipyrrolic fragment obtained from H_3(OEB). In addition, the tripyrrolic fragment $C_{26}H_{34}N_3O$, which corresponds to cleavage at the C14−C15 bond and contains no cyano groups, is observed at *m*/*e* 404.2659. Thus, the *meso*-cyano group must be at C15, on the same side of the verdin as the α-cyano group at C19.

Attempts to confirm that the yellow-green compound is H_2-(OEB-15,19-$(CN)_2$) and to characterize its novel structure by X-ray diffraction were thwarted by difficulties in growing of suitable crystals with the small amount of compound available. H_2(OEB-15,19-$(CN)_2$) is readily soluble in a wide range of solvents including hexane, ether, chloroform, methanol, and acetone. Crystals grown by diffusion of water into acetone were extensively twinned. Preparation of zinc complexes by nucleophilic addition of cyanide anion to [Zn^{II}(OEOP)]$^+$ offered the promise of cyanoverdin compounds that would be available in greater quantity and more readily crystallized.

Synthetic Studies of Cyanide Addition to Zinc Verdoheme, [Zn^{II}(OEOP)](O_2CCH_3). The results of addition of cyanide ion to the zinc verdoheme, [Zn^{II}(OEOP)](O_2CCH_3), and related compounds are summarized in Scheme 4. Surprisingly, the reaction results in substitution of one or two cyano groups at meso positions as well as the introduction of a cyano group at C19. The substitution is regioselective and affords the mono-*meso*-cyano-substituted regioisomer that is identical to the one isolated from the iron chemistry.

Addition of tetra(*n*-butyl)ammonium cyanide to [Zn^{II}-(OEOP)](O_2CCH_3) produces a mixture of at least three products: H_2(OEB-15,19-$(CN)_2$), Zn^{II}(OEB-15,19-$(CN)_2$), and Zn^{II}-(OEB-10,15,19-$(CN)_3$). The color of the reaction solution changes from the blue-green of the verdoheme complex (trace A of Figure 1) to an intermediate yellow-green, which then changes to brown upon washing with water. Thin-layer chromatography of the product mixture on silica with dichloromethane results in the separation of H_2(OEB-15,19-$(CN)_2$), Zn^{II}(OEB-15,19-$(CN)_2$), and Zn^{II}(OEB-10,15,19-$(CN)_3$). The yields of these three compounds are variable. Conditions were not found that led to either *meso*-cyano substitution exclusively at C15 or complete substitution at both C10 and C15. The reaction is most useful and reliable for the preparation of H_2-(OEB-15,19-$(CN)_2$), which is the first compound to elute during chromatography. Pure samples of Zn^{II}(OEB-15,19-$(CN)_2$) and Zn^{II}(OEB-10,15,19-$(CN)_3$) are difficult to obtain from the product mixture because chromatographic separation can be incomplete and the complexes cocrystallize. Indeed, Zn^{II}(OEB-10,15,19-$(CN)_3$) was discovered when disorder was observed during attempts to determine the X-ray crystal structure of Zn^{II}-(OEB-15,19-$(CN)_2$). The disorder could be modeled by partial occupancy of the site by a molecule with a third cyano group at C10.

The UV/vis spectra of these three compounds are shown in traces B, C, and D of Figure 1. The spectrum of H_2(OEB-15,-19-$(CN)_2$) strongly resembles that of Zn^{II}(OEBOMe), which has λ_{max} of 402, 710 sh, and 790 nm. The UV/vis spectra of Zn^{II}-(OEB-15,19-$(CN)_2$) and Zn^{II}(OEB-10,15,19-$(CN)_3$) have similar features, but the spectrum of Zn^{II}(OEB-10,15,19-$(CN)_3$) is red-shifted with respect to the spectrum of Zn^{II}(OEB-15,19-$(CN)_2$). The overall spectral patterns for Zn^{II}(OEB-15,19-$(CN)_2$) and Zn^{II}(OEB-10,15,19-$(CN)_3$) resemble the spectral patterns seen for the related helical complexes Zn^{II}(OEBOMe), Zn^{II}(OEB-SMe), and Zn^{II}(OEBNMe$_2$),[12,13] except for the presence of additional broad shoulders in the 500−600 nm region in the spectra of Zn^{II}(OEB-15,19-$(CN)_2$) and Zn^{II}(OEB-10,15,19-$(CN)_3$).

A synthetic route to introduce the 10-cyano substituent prior to cyanide addition to the zinc verdoheme was developed in an effort to prepare samples of the 10,15,19-tricyano complex Zn^{II}-(OEB-10,15,19-$(CN)_3$) in higher yield and purity. This, in turn, might serve to eliminate disorder in X-ray structure determinations. The previously reported compound H_3(OEB-10-(CN)) is obtained by treating H_3(OEB) with cyanide ion in dimethyl sulfoxide solution.[16] Insertion of zinc(II) into H_3(OEB-10-(CN)) produces Zn^{II}(HOEB-10-(CN)), which was isolated as green

(16) Falk, H.; Schlederer, T. *Monatsh. Chem.* **1978**, *109*, 1013.

Scheme 4

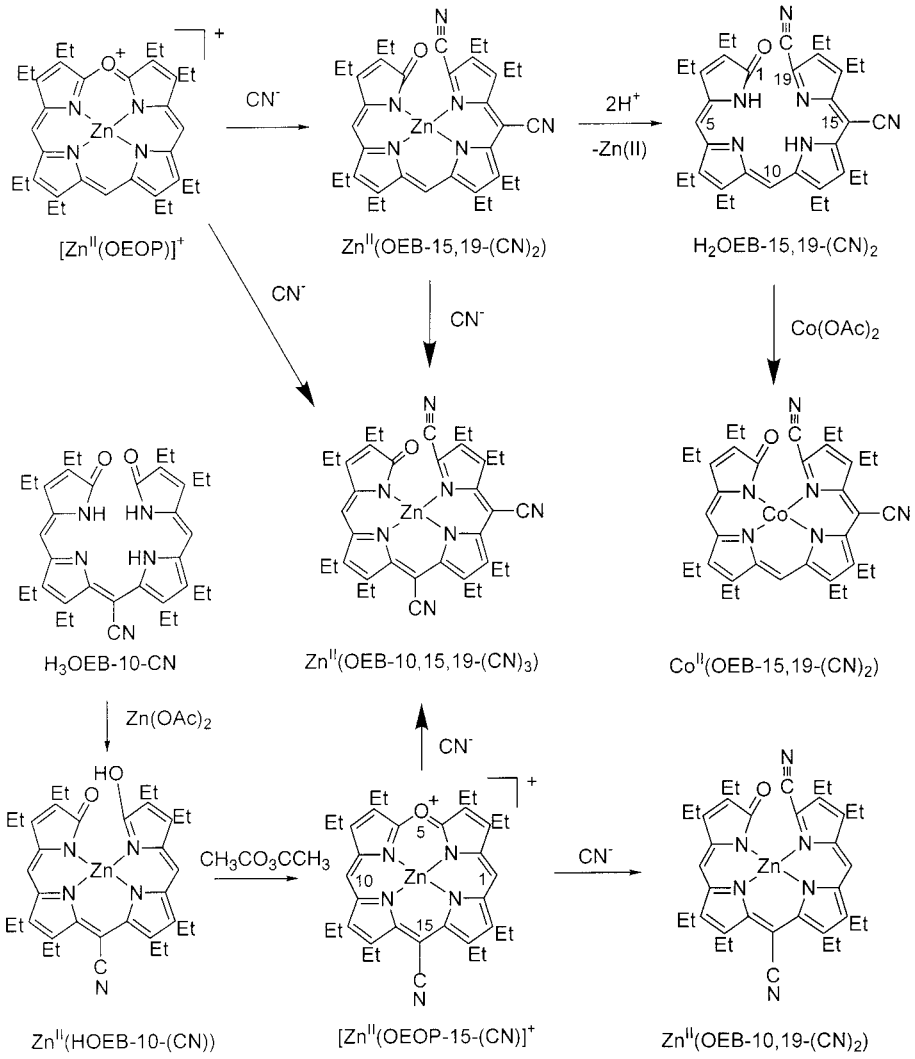

solid. The UV/vis spectra of H_3(OEB-10-(CN)) and Zn^{II}(HOEB-10-(CN)) are shown in traces A and B of Figure 2, respectively. As expected, metal ion insertion is accompanied by a red shift in the spectra. Zn^{II}(HOEB-10-(CN)) undergoes ring closure in the presence of acetic anhydride to give the verdoheme analogue [Zn^{II}(OEOP-15-(CN))](O_2CCH_3), whose UV/vis spectrum is shown in trace C of Figure 2. (Note: the change in the numbering of the meso positions is a consequence of a shift in origin in the numbering conventions for verdins and oxaporphyrins, see Scheme 2.) This complex has a characteristic verdoheme spectrum with a strong absorption at 690 nm. [Zn^{II}(OEOP-15-(CN))](O_2CCH_3) ring-opens when treated with cyanide, as shown in Scheme 3, to give mixtures of Zn^{II}(OEB-10,15,19-$(CN)_3$) and a fourth ring-opened complex, Zn^{II}(OEB-10,19-$(CN)_2$). The composition of the mixture can be varied by changing solvents and time of reaction. Zn^{II}(OEB-10,19-$(CN)_2$) was purified by column chromatography (see Experimental Section) and isolated as a dark brown solid. The UV/vis spectrum of Zn^{II}(OEB-10,19-$(CN)_2$) shows characteristics similar to those of Zn^{II}(OEB-15,19-$(CN)_2$) and Zn^{II}(OEB-10,-15,19-$(CN)_3$) with absorption at 426 and 900 nm as shown in trace D of Figure 2.

The ^{1}H NMR spectra (see Experimental Section for details) of these zinc compounds are consistent with their structures. For each compound, complex multiplets are observed in the regions 2.5−2.0 ppm and 1.2−0.8 ppm for the methylene and methyl protons of the ethyl groups, respectively. The downfield regions, which contain the meso resonances, are the most informative. The spectrum of the verdoheme [Zn^{II}(OEOP-15-(CN))](O_2CCH_3) shows, as expected for the symmetrical structure, a single resonance at 9.24 ppm for the two meso protons. The spectra of the isomeric Zn^{II}(OEB-15,19-$(CN)_2$) and Zn^{II}(OEB-10,19-$(CN)_2$) show two equally intense meso resonances at 5.9 and 6.4 ppm for Zn^{II}(OEB-15,19-$(CN)_2$) and at 5.86 and 6.94 ppm for Zn^{II}(OEB-10,19-$(CN)_2$). As expected, Zn^{II}(OEB-10,15,19-$(CN)_3$) displays only a single meso resonance at 6.12 ppm.

The Crystal and Molecular Structures of μ-H_2O-{Zn^{II}-(OEB-10,19-$(CN)_2$)}$_2$·0.5acetone·0.6H_2O and μ-H_2O-{(Zn^{II}-(OEB-10,15,19-$(CN)_3$)}$_2$·acetone. Crystals of μ-H_2O-{Zn^{II}-(OEB-10,19-$(CN)_2$)}$_2$·0.5acetone·0.6H_2O and μ-H_2O-{(Zn^{II}(OEB-10,15,19-$(CN)_3$)}$_2$·acetone were grown by layering water over a saturated acetone solution of Zn^{II}(OEB-10,19-$(CN)_2$) or Zn^{II}-(OEB-10,15,19-$(CN)_3$), respectively. Although the two complexes crystallize in different space groups (*Pbcn* for μ-H_2O-{Zn^{II}(OEB-10,19-$(CN)_2$)}$_2$ and *C*2/*c* for μ-H_2O-{(Zn^{II}(OEB-10,15,19-$(CN)_3$)}$_2$), the structures of the two binuclear complexes are remarkably similar. The most significant difference between the two structures is the presence of two cyano groups (per biliverdin) in μ-H_2O-{Zn^{II}(OEB-10,19-$(CN)_2$)}$_2$ and three (per biliverdin) in μ-H_2O-{(Zn^{II}(OEB-10,15,19-$(CN)_3$)}$_2$). In addition, the structure of μ-H_2O-{Zn^{II}(OEB-10,19-$(CN)_2$)}$_2$ is

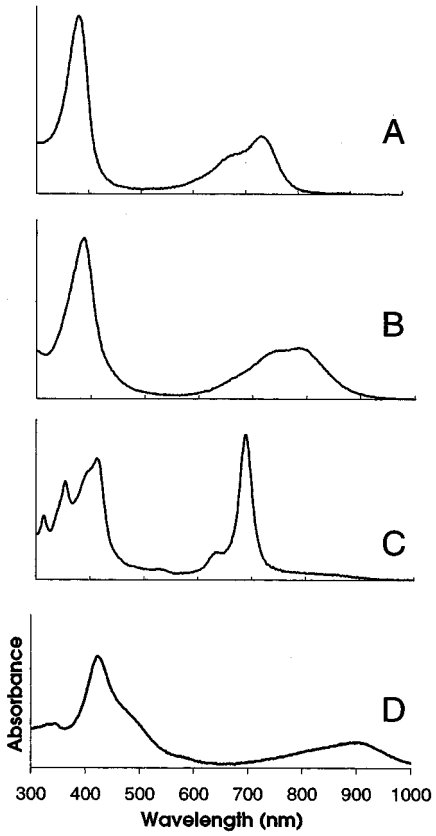

Figure 2. Electronic absorption spectra of chloroform solutions of (A) H_3OEB-10-CN [λ_{max}, nm (ϵ, M^{-1} cm^{-1}): 380 (50000), 680 (10000), 726 (15000)]; (B) Zn^{II}(HOEB-10-CN) [λ_{max}, nm (ϵ, M^{-1} cm^{-1}): 388 (50300), 790 (18600)]; (C) $[Zn^{II}(OEOP)\text{-}15\text{-}CN]^{+}(O_2CCH_3)$ [λ_{max}, nm (ϵ, M^{-1} cm^{-1}): 388 (50300), 790 (18600)]; and (D) Zn^{II}(OEB-10,19-$(CN)_2$) [λ_{max}, nm (ϵ, M^{-1} cm^{-1}): 422 (65000), 896 (13100)].

disordered so that there is partial occupancy (0.17) of a cyano substituent at C15. Figure 3 shows a drawing of the structure of μ-H_2O-{Zn^{II}(OEB-10,19-$(CN)_2$)}$_2$ with the ethyl groups removed so that the core structure is more readily appreciated. Figure 4 shows a perspective view of μ-H_2O-{(Zn^{II}(OEB-10,-15,19-$(CN)_3$)}$_2$ with the ethyl groups included. The disposition of ethyl groups seen in this drawing is also the one observed in μ-H_2O-{Zn^{II}(OEB-10,19-$(CN)_2$)}$_2$. Selected interatomic distances and angles for both binuclear complexes are presented in Table 1.

The structures of both μ-H_2O-{Zn^{II}(OEB-10,19-$(CN)_2$)}$_2$ and μ-H_2O-{(Zn^{II}(OEB-10,15,19-$(CN)_3$)}$_2$ consist of two tetrapyrrole subunits that are coordinated to zinc through four Zn−N bonds. The ligand in each monomeric portion has a helical geometry, which is similar to that of a number of other complexes of open-chain tetrapyrrole ligands. Particularly relevant examples of these include four-coordinate Zn^{II}(OEBOMe)[12] and Zn^{II}(OEB-NMe_2),[13] and five-coordinate $(H_2O)Zn^{II}$(OEFB).[17] The helical units, {Zn^{II}(OEB-10,19-$(CN)_2$)} or {(Zn^{II}(OEB-10,15,19-$(CN)_3$)}, are combined into the binuclear molecules by coordination of each zinc ion to a bridging water molecule. The bridging water molecule is also hydrogen-bonded to a lactam oxygen atom at one end of each tetrapyrrole subunit. The oxygen atom of the bridging water molecule in each of the two structures resides on a crystallographic 2-fold axis. Thus, each binuclear zinc complex is chiral, and both of the two helical tetrapyrrole units within any one binuclear complex have the same chirality.

(17) Struckmeier, G.; Thewalt, U.; Fuhrhop, J.-H. *J. Am. Chem. Soc.* **1976**, *98*, 278.

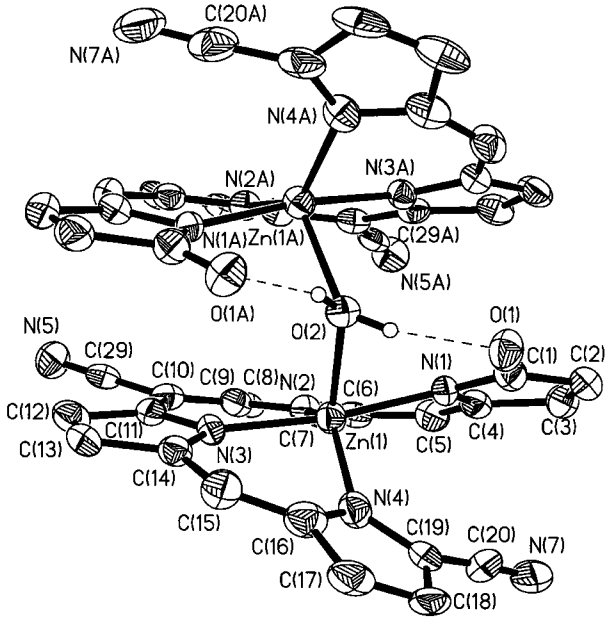

Figure 3. A perspective view of μ-H_2O-{Zn^{II}(OEB-10,19-$(CN)_2$)}$_2$ showing the numbering scheme and 50% thermal ellipsoids. The ethyl groups are removed to emphasize the helical nature of the inner core. There is a cyano group with 0.17 partial occupancy attached at C15 which also is not shown.

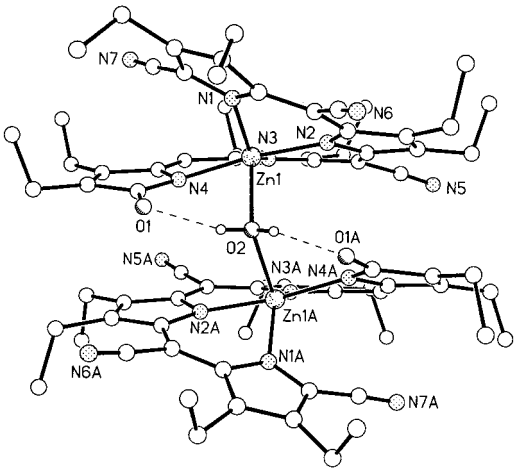

Figure 4. A perspective view of μ-H_2O-{(Zn^{II}(OEB-10,15,19-$(CN)_3$)}$_2$ showing the numbering scheme and 50% thermal ellipsoids. The ethyl groups are included.

However, both of the binuclear complexes crystallize in centrosymmetric space groups. Consequently, each crystal contains a racemic mixture of the binuclear complexes.

The coordination geometry of each zinc atom in μ-H_2O-{Zn^{II}-(OEB-10,19-$(CN)_2$)}$_2$ approximates a trigonal bipyramid. The axial portion is composed of the N(1)−Zn−N(3) segment, which has a nearly linear geometry (bond angle, 172.1(2)°). Within the equatorial plane, the N(2)−Zn−N(4) and O(2)−Zn−N(2) angles (138.1(3)° and 126.1(2)°, respectively) are wider than the expected 120°. The O(2)−Zn−N(4) angle of 95.8(2)° is narrower than the expected value. The sum of these three bond angles is 360°, so the ZnO(2)N(2)N(4) unit is planar. The bond angles at the zinc between the axial and equatorial donors fall into a reasonably narrow range, 83.8−98°, that is near the ideal of 90°. The bridging water is of particular note. The Zn(1)−O(2)−Zn(2) angle of 109.8(3)° is near the expected value of 109.5° for tetrahedral geometry, and the O(2)−H(2) distance is in the range typical of hydrogen bonding.

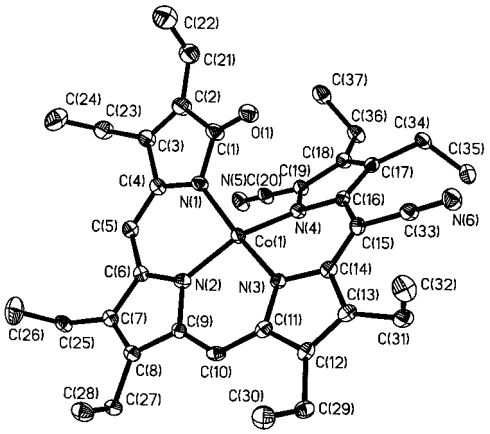

Figure 5. A perspective view of Co^{II}(OEB-15,19-$(CN)_2$) showing a numbering scheme and 50% thermal contours for all atoms. The hydrogen atoms were removed for clarity.

Table 1. Selected Bond Lengths (Å) and Bond Angles (deg) for μ-H_2O-{Zn^{II}(OEB-10,15,19-$(CN)_3$)}$_2$, μ-H_2O-{Zn^{II}(OEB-10,19-$(CN)_2$)}$_2$, and Co^{II}(OEB-15,19-$(CN)_2$)

	μ-H_2O-{Zn^{II}(OEB-10,19-$(CN)_2$)}$_2$	μ-H_2O-{Zn^{II}(OEB-10,15,19-$(CN)_3$)}$_2$	Co^{II}(OEB-15,19-$(CN)_2$)
	Bond Lengths (Å)		
M−N(1)	2.029(6)	2.0254(15)	1.854(3)
M−N(2)	2.040(6)	2.0048(15)	1.882(3)
M−N(3)	2.039(5)	2.0186(14)	1.872(3)
M−N(4)	2.054(6)	2.0263(16)	1.888(3)
M−O(2)	2.222(4)	2.2685(11)	
O(2)−H···O(1)	1.86(3)	2.011(14)	
C(1)−O(1)	1.229(9)	1.236(2)	1.212(4)
C(19)−C(20)	1.401(13)	1.433(3)	1.433(4)
	Bond Angles (deg)		
N(1)−M−N(2)	88.8(2)	89.91(6)	91.21(12)
N(1)−M−N(3)	172.1(2)	173.45(6)	166.45(11)
N(1)−M−N(4)	98.0(2)	97.80(6)	92.73(12)
N(2)−M−N(3)	87.8(2)	89.66(6)	94.01(11)
N(2)−M−N(4)	138.1(2)	135.31(6)	148.12(11)
N(3)−M−N(4)	89.3(2)	87.08(7)	89.44(11)
M−O(2)−M′	109.8(3)	110.62(8)	

Each zinc atom in μ-H_2O-{(Zn^{II}(OEB-10,15,19-$(CN)_3$)}$_2$ is also five-coordinate with trigonal bipyramidal geometry. Inspection of Table 1 reveals that the differences in the coordination geometry of μ-H_2O-{(Zn^{II}(OEB-10,15,19-$(CN)_3$)}$_2$ and μ-H_2O-{Zn^{II}(OEB-10,19-$(CN)_2$)}$_2$ are small.

Synthesis of Co^{II}(OEB-15,19-$(CN)_2$). Since efforts to obtain crystals of Zn^{II}(OEB-15,19-$(CN)_2$) did not meet with success, the corresponding cobalt complex, Co^{II}(OEB-15,19-$(CN)_2$), was prepared and crystallized. Co^{II}(OEB-15,19-$(CN)_2$) was prepared by treating H_2(OEB-15,19-$(CN)_2$) with cobalt(II) acetate. Co^{II}-(OEB-15,19-$(CN)_2$), a somewhat air-sensitive compound when allowed to stand in solution, has UV/vis spectral features (λ_{max}, 440 nm, 796 nm) very similar to those previously reported for Co^{II}(OEFB).[15]

The Crystal and Molecular Structure of Co^{II}(OEB-15,-19-$(CN)_2$)·acetone. A perspective view of this complex is shown in Figure 5. The structure clearly shows the presence of cyano substituents at the 15 and 19 positions of the open-chain tetrapyrrole. The cobalt ion is four-coordinate and can best be described as having a flattened tetrahedral shape with bond angles, internal to the chelate, that approach 90°. In contrast to Zn^{II}(OEB-10,19-$(CN)_2$) and Zn^{II}(OEB-10,15,19-$(CN)_3$), the cobalt ion shows no affinity for water as an additional ligand and shows structural features that are similar to those of Co^{II}-(OEFB).[15] The ligand in Co^{II}(OEB-15,19-$(CN)_2$) adopts a helical structure in order to relieve steric constraints imposed by the terminal keto and cyano functionalities. Since the ligand is no longer constrained to a macrocyclic environment, radial contraction about the cobalt can occur, and the Co−N distances shorten. Thus the Co−N distances (1.854(3), 1.872(3), 1.882(3), and 1.888(3) Å) in Co^{II}(OEB-15,19-$(CN)_2$) are shorter than those of corresponding cobalt(II) porphyrins. For example, the Co−N distances in Co^{II}(OEP) are 1.967(3) and 1.975(3) Å.[18]

Theoretical Studies. A series of DFT geometry optimization calculations were performed on zinc complexes of 5-oxaporphyrins (verdoheme), verdins (bilindione), 4-cyano-5-oxaporphyrins, and 19-cyanoverdins in an effort to gain insights to the features of these complexes and the reactions that lead to *meso*-cyano-substituted cyanoverdins. Because zinc potentially could be four- or five-coordinate in solution, the series included complexes in which zinc had no additional axial ligand, a neutral axial water ligand, or an anionic axial cyanide ligand. Hydrogen atoms were used in place of β-alkyl substituents in order to decrease the already considerable computational challenge of the optimizations and to speed convergence by eliminating side chain conformations. Complexes with *meso*-cyano substituents at C10 and C15 were also examined. Starting geometries were obtained from a graphical builder rather than from X-ray coordinates, with the exception of the μ-H_2O-{(Zn^{II}(OEB-10,-15,19-$(CN)_3$)}$_2$ complex. Some of the results of the calculations are summarized in Tables 2 and 3.

The structural parameters calculated for the zinc oxaporphyrin complexes are in good agreement with corresponding parameters observed in the X-ray structures reported for this class of complexes.[4,5,8,9,15,19,20] The oxaporphyrin units of both series of complexes are planar and show near 2-fold symmetry with respect to the C15−M−O axis. Unfortunately, most reported oxaporphyrin structures display orientational disorder that involves multiple sites for the *meso*-oxa group, which obscures small variations in bond lengths in regions near the disordered oxa group. One structure with an ordered oxaporphyrin unit is that of [(OEOP)Co^{II}](PF_6)·CH_2Cl_2.[5] The oxa group of the complex has two C−O bond distances that are indistinguishable and average 1.344 Å and a C−O−C bond angle of 124.8°. Calculated values agree within 0.01 Å and 1.0°, respectively, values that are $\leq 2\sigma$ for the X-ray structure determination. The Co structure shows some alternation of bond lengths in the inner conjugation pathway in the half of the molecule that contains the oxa group. The C6−N2 bond, which is adjacent to the oxa group, is roughly 0.06 Å shorter than the C9−N2 bond in the same pyrrole ring, and the C9−C10 bond is roughly 0.02 Å shorter than the C10−C11 bond. These differences are reproduced in the calculated structures. The one reported structure of a zinc oxaporphyrin complex, that of [Zn(oxa-mesoporphyrin dimethyl ester)Cl], was of limited quality due to poor crystal quality, limited data, and side-chain disorder.[20] Hence, the markedly different bond lengths of the oxa group (1.26 and 1.37 Å) and the large alternation in bond lengths (∼0.1 Å) in the inner conjugation pathway of the molecule, features not observed in other reported oxaporphyrin structures, may be suspect. Nonetheless, the Zn−N bond lengths and the 0.54 Å out-of-plane displacement of the Zn atom are in good agreement with those in the calculated structure of the five-coordinate complex [Zn(oxaporphyrin)CN]. The calculated Zn−N bond lengths are smaller in [Zn(oxaporphyrin)(H_2O)]$^+$, which has a neutral axial ligand, and smallest in the four-coordinate [Zn(oxaporphyrin)]$^+$,

(18) Scheidt, W. R.; Turowska-Tyrk, I. *Inorg. Chem.* **1994**, *33*, 1314.
(19) Balch, A. L.; Noll, B. C.; Safari, N. *Inorg. Chem.* **1993**, *32*, 2901.
(20) Fuhrhop, J.-H.; Krüger, P.; Sheldrick, W. S. *Justus Liebigs Ann. Chem.* **1977**, 339.

Table 2. Results of Density Functional Theory Calculations on Zn(tetrapyrrole)L Complexes[a]

tetrapyrrole	substituent[b]	L	charge	$E^{c,d}$	HOMO[c]	LUMO[c]
5-oxaporphyrin			+1	−2792.87103	−0.34222	−0.28057
	15-CN		+1	−2884.37193	−0.35339	−0.29548
		H_2O	+1	−2868.80603	−0.33363	−0.27159
		CN	0	−2885.15712	−0.21584[e]	−0.16139
verdin			−1	−2867.92060	−0.05425	−0.01815
		H_2O	−1	−2943.86410	−0.05433	−0.01760
4-cyano-5-oxaporphyrin			0	−2885.16439	−0.18853	−0.14775
	15-CN		0	−2976.67833	−0.20207	−0.16445
		H_2O	0	−2961.09455	−0.18245	−0.14343
	15-CN	H_2O	0	−3052.60905	−0.19663	−0.15967
		CN	−1	−2977.33423	−0.06870	−0.03550
19-cyanoverdin			0	−2885.17936	−0.19984	−0.16428
	10-CN		0	−2976.69067	−0.21371	−0.17994
		H_2O	0	−2961.12722	−0.19919	−0.16025
	10-CN	H_2O	0	−3052.64021	−0.21224	−0.17645
	10,15-$(CN)_2$	H_2O	0	−3144.14812	−0.22349	−0.19060
		CN	−1	−2977.34179	−0.08056	−0.04871

[a] Local density functional theory calculations using VWN exchange-correlation with DN** basis. [b] Location of substituent on tetrapyrrole ligand referred to numbering scheme for that ligand system. [c] Energies in hartree units. [d] Results for water and cyanide anion are −75.90755 h and −92.08570 h, respectively. [e] Unlike other complexes, HOMO is centered on axial CN ligand.

Table 3. Calculated Energy Change for Ring-Openings of Zn(19-cyanoverdin)L

substituent[a]	L	ΔE (kcal/mol)
		−9.39
10-CN	−	−7.74
	H_2O	−20.5
10-CN	H_2O	−19.5
	CN	−4.74

[a] Position of substituent in cyanoverdin product.

which has no axial ligand. The out-of-plane displacements of the zinc atoms in the latter two complexes, which are 0.25 and 0.00 Å, respectively, are also smaller than that in the complex with the axial cyanide ligand.

The calculated charge distributions and frontier orbitals of the zinc oxaporphyrin complexes are consistent with Mulliken population analysis and orbital contributions previously obtained from semiquantitative Fenske−Hall LCAO molecular orbital calculations on the oxaporphyrin anion.[8] Unlike the Mulliken charges, though, charges determined by fits to the electrostatic potential establish that the valley carbons (C4 and C6) adjacent to the oxa group in the three zinc complexes have markedly greater positive charge than any other atom in the complex, including the zinc atoms (0.37−0.52 for C4 vs 0.19−0.24 for Zn). Experimentally, the valley carbons are the sites most susceptible to nucleophilic attack. The Fenske−Hall HOMO and LUMO resemble those calculated for the Zn complexes, but orbital energies and relative contributions of atomic orbitals differ. One exception is the cyanide complex, whose HOMO is primarily centered on the axial cyanide ligand.

The calculated structure of the four-coordinate zinc verdin anion reproduced the general features observed in helical, four-coordinate metal complexes of verdins, but detailed comparisons are complicated because the state of verdin protonation and the metal and verdin oxidation states are not entirely certain in these complexes.[21−24] The two interior pyrrole rings adjacent to C10 and the zinc atom are coplanar within 0.15 Å. The two five-membered lactam rings (the C19−OH group is deprotonated in the zinc verdin complex) are individually planar, but canted with respect to the rest of the structure to give the verdin ligand an overall helical conformation. An unexpected feature of the five-coordinate complex is hydrogen bonding between the axial water ligand and the oxygen atom of one lactam. The complex is approximately trigonal bipyramidal at zinc. The N_A atom of the hydrogen-bonded lactam ring and the opposite pyrrole ring occupy the axial coordination sites ($N_A-Zn-N_C = 164.7°$), and the remaining N atoms and the coordinated water occupy equatorial sites, whose bond angles ($N_B-Zn-N_D = 139.4°$, $N_B-Zn-O = 129.1°$, and $N_D-Zn-O = 91.3°$) deviate from the idealized 120°. Several starting geometries that had different orientations of non-hydrogen-bonded axial water ligands converged to this structure. It is noteworthy that the LUMOs of both complexes have a large amplitude at C10. Many examples of nucleophile addition at C10 of verdins have been reported.[16,25,26] Also noteworthy is the relatively instability (high energy) of the HOMO of these complexes as seen in Table 3. Free-base verdins and their metal complexes are known to be readily susceptible to oxidation.[24,27−29]

Calculations establish that addition of cyanide anion to the valley carbon of zinc oxaporphyrin complexes affords zinc 4-cyano-5-oxaporphyrin complexes that are stable relative to the starting complex and free cyanide. The structural features around the site of addition change to reflect the sp^3 hybridization of carbon atom C4 in the adduct. The C4−N1, C4−C3, and C4−O bond distances lengthen to 1.43, 1.50, and 1.42−1.43 Å, respectively. Bond angles about C4 are close to 109°, with the exception of 105.1° in the five-membered pyrrole ring and 114.6° in the adjacent six-membered ring. The cyanide group is canted somewhat from perpendicular to the oxaporphyrin ring, which deviates from planarity in the region of C4 and O. The C4−O−C6 bond angle decreases to 116° to accommodate these deviations. The HOMO of the adduct, which has a large

(21) Bonfiglio, J. V.; Bonnett, R.; Buckley, D. G.; Hamzetash, D.; Hursthouse, M. B.; Malik, K. M. A.; McDonagh, A. F.; Trotter, J. *Tetrahedron* **1983**, *39*, 1865.
(22) Balch, A. L.; Mazzanti, M.; Noll, B. C.; Olmstead, M. M. *J. Am. Chem. Soc.* **1993**, *115*, 12206.
(23) Balch, A. L.; Mazzanti, M.; Noll, B. C.; Olmstead, M. M. *J. Am. Chem. Soc.* **1994**, *116*, 9114.
(24) Lord, P. A.; Olmstead, M. M.; Balch, A. L. *Inorg. Chem.* **2000**, *39*, 0000.
(25) Falk, H.; Müller, N.; Schlederer, T. *Monatsh. Chem.* **1980**, *111*, 159.
(26) Falk, H.; Marko, H. *Monatsh. Chem.* **1991**, *122*, 319.
(27) Attar, S.; Ozarowski, A.; Van Calcar, P. M.; Winkler, K.; Balch, A. L. *Chem. Commun.* **1997**, 1115.
(28) Balch, A. L.; Koerner, R.; Olmstead, M. M.; Mazzanti, M.; Safari, N.; St. Claire, T. *J. Chem. Soc., Chem. Commun.* **1995**, 643.
(29) Attar, S.; Balch, A. L.; Van Calcar, P. M.; Winkler, K. *J. Am. Chem. Soc.* **1997**, *119*, 3317

amplitude at C20 and somewhat lesser amplitude at C15, is significantly destabilized in the adduct relative to the oxaporphyrin.

The structures calculated for the 19-cyanoverdin complexes are similar to those of the verdin complexes except for the replacement of the hydroxyl group at C19 with a cyano group. The cyanoverdin ligand adopts a helical conformation around the zinc atom, which has a distorted trigonal bipyramidal geometry in the five-coordinate water and cyanide complexes. Hydrogen bonding occurs between the coordinated water and the remaining carbonyl oxygen at C1 in the water complex. The HOMO of the cyanoverdin is also destabilized relative to the oxaporphyrin, but is more stable than that of the 4-cyano-5-oxaporphyrin. In contrast to the latter, the HOMO of the cyanoverdin has large amplitude at C5, the meso carbon adjacent to the lactam ring.

The total energies of the 19-cyanoverdin complexes are more negative than the energies of the corresponding 4-cyano-5-oxaporphyrin complexes. The energy by which the cyanoverdin complexes are favored at equilibrium is presented in Table 3. Formation of a hydrogen bond in the 5-coordinate aquo complex of the cyanoverdin certainly helps drive the conversion. Data for the four-coordinate complex and 5-coordinate cyanide complex suggest, though, that the conversion is spontaneous without the added stability of the hydrogen bond. Comparisons of the structure of the complexes, Figure 6, suggest that activation barriers to conversion could be significant. The C4−O distance must increase from 1.42 Å in the 4-cyano-5-oxaporphyrin to between 3.25 and 3.8 Å in the cyanoverdin. The cyano group moves from off perpendicular to coplanar with the five-membered pyrrole ring upon rehybridization of the carbon from sp^3 to sp^2. Finally, significant changes must occur in the coordination geometry about zinc and in the conformation of the ligand.

Substitution of cyano groups at the meso positions of the series of complexes had limited effects. The $C_\alpha-C_M$ bond lengths to the substituted meso carbon increase slightly, and the $C_\alpha-C_M-C_\alpha$ bond angle decreases slightly. The energies of the HOMOs were stabilized by roughly 0.01−0.02 eV per cyano group. They resembled those of the unsubstituted complexes, but the amplitude of the wave function at the substituted meso carbon decreased.

An optimized geometry was calculated for a μ-H_2O-{(Zn^{II}-(OEB-10,15,19-$(CN)_3$)}$_2$ complex with starting coordinates obtained from the X-ray structure of μ-H_2O-{(Zn^{II}(OEB-10,-15,19-$(CN)_3$)}$_2$. To make the calculation tractable, C_2 symmetry was imposed, all ethyl group substituents were replaced with H atoms, and the acetone of solvation was omitted. The major differences between the optimized structure and the X-ray structure involved coordination of zinc by the bridging water ligand and the hydrogen bond between this water and the carbonyl oxygen. Both interactions strengthened in the optimized structure. The Zn−O distance decreased from 2.269 to 2.179 Å, the H−O distance in the hydrogen bond decreased from 2.010 to 1.579 Å, and the Zn−O−Zn bond angle decreased from 110.6° to 108.1°. These changes probably reflect relaxation of constraints imposed by the presence of the acetone of solvation, which occupies the space between the two cyanoverdin helices in the region of the bridging water ligand.

Discussion

The results presented here demonstrate that the addition of cyanide ion to [Zn^{II}(OEOP)](O_2CCH_3) is a more complex process than that observed when methoxide, methanethiolate, or dimethylamide are added to the same zinc verdoheme. Addition of these nucleophiles to [Zn^{II}(OEOP)](O_2CCH_3) proceeded in good yield to produce helical complexes of the ring-opened tetrapyrroles as shown in Scheme 2. In these cases there was no indication of further reaction of the nucleophile with the ring-opened tetrapyrrole. However, when cyanide reacts with [Zn^{II}(OEOP)](O_2CCH_3), ring-opening is accompanied by a degree of substitution at the meso positions. The reaction is reminiscent of the reaction of cyanide with H_3OEB which results in meso substitution and the formation of H_3(OEB-10-(CN)).[16] However, the reaction of cyanide with [Zn^{II}(OEOP)](O_2CCH_3) is difficult to control, and at least three products, H_2(OEB-15,-19-$(CN)_2$), Zn^{II}(OEB-15,19-$(CN)_2$), and Zn^{II}(OEB-10,15,19-$(CN)_3$), are formed. Clean separation of these products is difficult to achieve, and an alternate route to Zn^{II}(OEB-10,15,-19-$(CN)_3$) that utilizes H_3(OEB-10-(CN)) to afford more

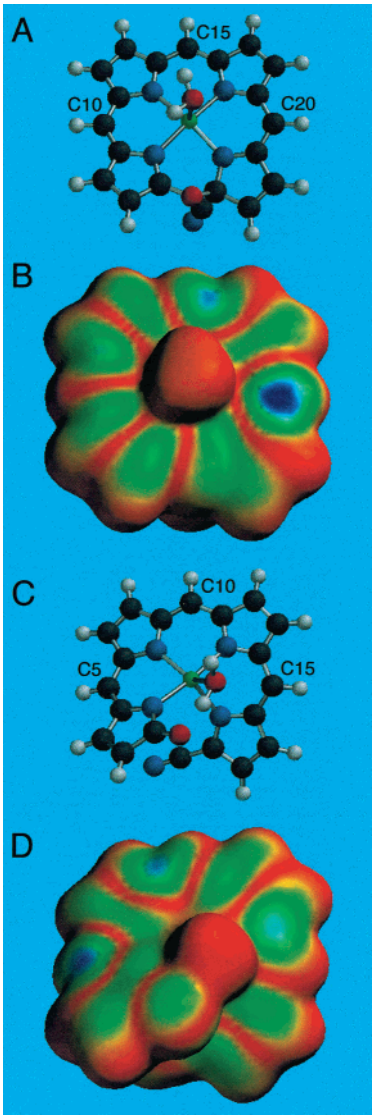

Figure 6. Comparisons of the calculated structures of (A) Zn(4-cyano-5-oxaporphyrin)(H_2O) and (C) Zn(19-cyanoverdin)(H_2O), and of the magnitude of the SOMO mapped onto the electron density surface (0.002 e/Å^3) of the cation radicals (B) Zn(4-cyano-5-oxaporphyrin)-$(H_2O)^+$ and (D) Zn(19-cyanoverdin)$(H_2O)^+$. The orientations of the molecules are identical in the pair A and B and in the pair C and D. The view in all structures is from the direction of the axial water ligand. Blue indicates a large value of the SOMO, and red is a zero value. The SOMO mappings for B and D are on the same absolute scale. Meso carbon numbers in A and B are indicated in the appropriate numbering system for the two different tetrapyrrole ligands.

Scheme 5

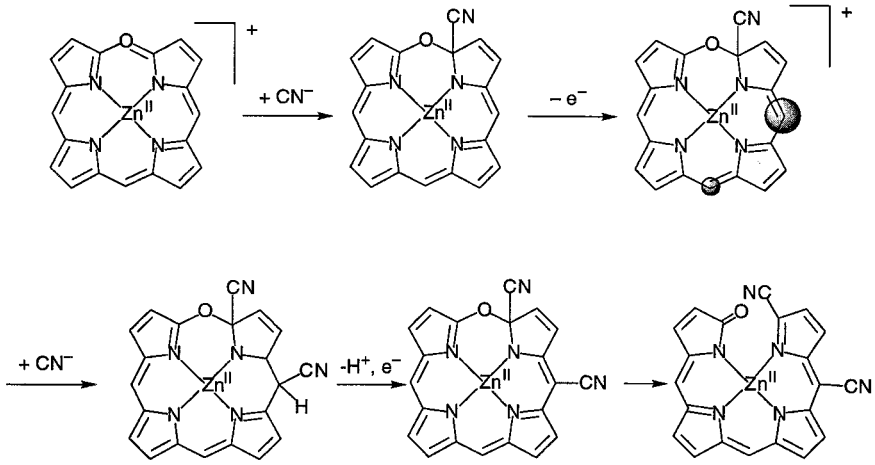

complete substitution at the 10-position has been devised. Substitution of the meso protons during this process appears to occur preferentially at the 15 position with additional substitution also occurring at the 10 position. Note that this preference differs from that observed with the free ligand H_3OEB, where substitution occurs preferentially at the 10 position.[16]

When crystallized from acetone/water, the binuclear complexes μ-H_2O-{Zn^{II}(OEB-10,19-$(CN)_2$)}$_2$ and μ-H_2O-{(Zn^{II}-(OEB-10,15,19-$(CN)_3$)}$_2$ are obtained. These complexes have helical structures in which the chirality of both tetrapyrroles is the same in any one molecule. The bridging water molecule, which is hydrogen bonded to both tetrapyrrole ligands, serves as an effective link that transfers the helical sense of one tetrapyrrole on to the adjacent tetrapyrrole. Consequently the entire binuclear complex is chiral for both compounds, μ-H_2O-{Zn^{II}(OEB-10,19-$(CN)_2$)}$_2$ and μ-H_2O-{(Zn^{II}(OEB-10,15,19-$(CN)_3$)}$_2$. However, each of these complexes crystallizes in a centrosymmetric space group, and hence each crystal is a racemate. It is likely that these five-coordinate binuclear complexes dissociate into four-coordinate monomers in solution. Prior crystallographic studies of Zn^{II}(OEBOMe), Zn^{II}(OEB-SMe), and Zn^{II}(OEBNMe$_2$) indicate that each exists as a four-coordinate monomer,[12,13] and we suspect that similar monomeric units are found in solution for the new complexes outlined in Scheme 4. Although zinc complexes of open and closed tetrapyrrole ligands can be either four- or five-coordinate, we have not been able to identify another example of a zinc tetrapyrrole complex that incorporates a bridging water molecule. A search of the Cambridge Structural Database shows the existence of only a single zinc complex, {(μ-H_2O)Zn(H_2O)-SO_4)(μ-hypoxanthininato)}$_2$, with bridging water molecule.[30]

The major questions raised by our experimental results are what is the mechanism of *meso*-cyano substitution in these reactions and why is the substitution regioselective. Cyanide ion is readily oxidized to cyanogen by transition metal ions including Cu(II) and Hg(II). In addition, ferric porphyrin complexes are known to autoreduce in the presence of excess cyanide to afford ferrous porphyrin biscyanide complexes and cyanide radical.[31] Thus, radical addition and/or substitution reactions might be possible during the coupled oxidation of iron porphyrin complexes in the presence of cyanide ion. However, Zn(II) is incapable of oxidizing cyanide. A more general mechanism for *meso*-cyano substitution is suggested by the DFT calculations and is shown in Scheme 4. Addition of cyanide to the valley carbon of the oxaporphyrin complex leads to a substantial increase in the energy of the HOMO of the resulting 4-cyano-5-oxaporphyrin complex. Oxidation of the complex by air or other oxidant would afford a radical whose singly occupied MO resembles the HOMO of the 4-cyano-5-oxaporphyrin complex. Calculations show the SOMO and spin density have greatest magnitude at C20 and a smaller magnitude at C15 (which correspond to C15 and C10, respectively, in the ring-open cyanoverdin). These are represented by the shaded circles at these sites in Scheme 5. Nucleophilic attack by a cyanide anion at these meso sites followed by oxidation and loss of the original meso proton would afford a *meso*-cyano-substituted 4-cyano-5-oxaporphyrin complex. A second cycle of oxidation, addition, and oxidation could afford a 4-cyano-5-oxaporphyrin complex with two *meso*-cyano substituents. Ring-opening would give the final cyanoverdin products with correct regioselectivity. The calculations further suggest that substitution does not occur by oxidation once the cyanoverdin complex has formed. Figure 6 compares the magnitudes of the SOMOs of the 4-cyano-5-oxaporphyrin radical and the 19-cyanoverdin radical mapped on their respective electron density surfaces. The SOMO of the cyanoverdin radical has greatest magnitude at C5 and would therefore afford the wrong regioisomeric product. Thus, meso substitution appears to be competitive with ring-opening, which we suggested above should have a non-negligible activation barrier. The kinetic complexity of the scheme helps rationalize the observed variability in product yields with small differences in reaction conditions. Precedent for the mechanism proposed in Scheme 5 can be found in a related mechanism involving nucleophilic attack on oxidatively generated verdin cations which has been suggested to explain the formation of 15,16-dimethoxybilindione compounds.[32,33]

Experimental Section

Preparation of Compounds. The preparations of H_3(OEB-10-(CN)) and [Zn^{II}(OEOP)](O_2CCH_3) were adapted from previously reported syntheses.[16,20] All solvents were used as purchased and used without further purification.

H_2(OEB-15,19-$(CN)_2$). Method 1. [Fe^{III}(OEP)]Cl (113 mg, 0.1181 mmol) was added to a solution of ascorbic acid (1.00 g, 5.68 mmol) and potassium cyanide (1.50 g, 23.0 mmol) in 200 mL of methanol. The mixture was stirred rapidly, but without turbulence, in air for 11 h. The resulting brownish green solution was evaporated to dryness

(30) Duber, E.; Hänggi, G.; Schmalle, H. *Inorg. Chem.* **1990**, *29*, 2518.
(31) Del Gaudio, J.; La Mar, G. N. *J. Am. Chem. Soc.* **1976**, *98*, 3014.
(32) Eivazi, F.; Hudson, M. F.; Smith, K. M. *Tetrahedron* **1977**, *33*, 2959.
(33) Eivazi, F.; Smith, K. M. *J. Chem. Soc., Perkin Trans. 1* **1979**, 544.

under reduced pressure. The residue was redissolved by treatment with 100 mL of dichloromethane and 100 mL of water. This mixture was transferred to a separatory funnel and washed with water (4 × 200 mL). Care was taken to allow emulsions which formed during the washes to break up before the layers were separated. The dichloromethane solution was separated, dried over anhydrous sodium sulfate, filtered, and evaporated under reduced pressure. A portion of the solid was dissolved in chloroform. The resulting solution was filtered through a membrane-type HPLC syringe filter onto a preabsorbent zone of a 20 × 20 cm Analtech 0.5 mm silica gel preparative TLC plate. The plate was developed with chloroform to give 10 resolved bands and an unresolved brown smear extending upward from the origin. The colors of the resolved bands on the dried plate in order of decreasing R_f were yellow, brown-yellow, yellow-green which contained H_2(OEB-15,19-(CN)$_2$), pink, purple-pink, peach, purple, blue, purple-gray, and red-violet. Fractions of the yellow-green band were scraped from the silica plate with a scalpel and extracted from the silica with chloroform. Multiple TLC separations were conducted to recover roughly 3 mg of H_2[OEB-15,19-(CN)$_2$]. UV−vis ($CHCl_3$): λ_{max}, nm (relative absorbances) 302 (0.83), 412 (1.00), 722 sh (0.25), 778 (0.33). ^{1}H NMR (CD_2Cl_2): δ 12.60 (br s, 1 H, NH), 8.81 (br s, 1 H, NH), 6.89 and 6.26 (s, 1 H each, 5,10-H), 3.10, 2.95, 2.75, 2.46, 2.28 (q, 2 H each, CH_2), 2.70−2.52 (m 6 H, CH_2), 1.40−1.19 (m, 18 H, CH_3), 1.15 and 1.06 (t, 3 H each, CH_3). MS (MALDI): *m*/*e* 611.3406 ($C_{37}H_{44}N_6O$ + Na^+), 585.3359 ($C_{36}H_{44}N_5O$ + Na^+, i.e., loss of CN), 416.2694 ($C_{27}H_{34}N_3O$), 404.2659 ($C_{26}H_{34}N_3O$), 283.1792 ($C_{18}H_{23}N_2O$).

H_2(OEB-15,19-(CN)$_2$). Method 2. [Zn^{II}(OEOP)](O_2CCH_3) (70 mg, 0.11 mmol) was dissolved in 30 mL of dichloromethane in a 100 mL flask and brought to reflux temperature. Tetra(*n*-butyl)ammonium cyanide (172 mg. 0.66 mmol) was added to the dichloromethane solution and the reaction mixture stirred for 30 min. A color change from green to yellow-green was observed during this time frame. The contents of the flask were poured into 70 mL of dichloromethane and then extracted with water (4 × 100 mL). The dichloromethane layer was observed to change from a yellow-green to a brown-green. This layer was separated, dried with sodium sulfate, and taken to dryness to give an olive-green solid. Column chromatography of this solid on silica (3 × 20 cm), with 2% tetrahydrofuran in dichloromethane, produced many different colored bands. The first major band, yellow-green H_2(OEB-15,19-(CN)$_2$), was isolated and repurified by column chromatography on silica (3 × 15 cm) with 10% tetrahydrofuran in hexanes. The second major band, brown Zn^{II}(OEB-10,15,19-(CN)$_3$), was also collected and repurified by column chromatography on silica (3 × 15 cm) with 10% tetrahydrofuran in hexanes (characterization provided below). A third major band, brown Zn^{II}(OEB-15,19-(CN)$_2$), was collected and repurified by column chromatography on silica (3 × 15 cm) with 10% tetrahydrofuran in hexanes (characterization provided below). Two remaining purple fractions were not identified. Yield: 9.5 mg, 15%. UV/vis spectrum in chloroform [λ_{max}, nm, (ϵ, M^{-1} cm^{-1})]: 302 (21700), 416 (26200), 724 (7100), 774 (9300). 300 MHz ^{1}H NMR (chloroform-*d*): 12.61 (br s, 1 H, N*H*), 8.86 (br s, 1 H, N*H*), 6.82 and 6.26 (s, 1 H each, 5,10-*H*), 3.20−2.20 (m 16 H, CH_2), 1.50−1.00 (m, 24 H, CH_3).

Zn^{II}(OEB-10,15,19-(CN)$_3$). The isolation of this compound was described above in the synthesis of H_2(OEB-15,19-(CN)$_2$) as the second major band (brown). Yield: 4.4 mg, 6.1%. UV/vis spectrum in chloroform [λ_{max}, nm (ϵ, M^{-1} cm^{-1})]: 444 (13700), 906 (3480). 400 MHz ^{1}H NMR (chloroform-*d*): δ 6.12 (s, 1 H, 5-*H*), 2.90 (m, 4 H, CH_2), 2.50 (m, 12 H, CH_2), 1.15 (m, 24 H, CH_3). IR (Fluorolube mull, cm^{-1}): 2970 s, 2930 s, 2880 m, 2850 m, 2210 w (ν(CN)), 1720 w, 1670 w, 1550 s, 1500 m, 1460 m, 1380 m. MS (MALDI): *m*/*e* 676.24 (M^+) ($C_{38}H_{41}N_7OZn^+$).

Zn^{II}(OEB-15,19-(CN)$_2$). The isolation of this compound was described above in the synthesis of H_2(OEB-15,19-(CN)$_2$) as the third major band (brown). Yield: 10 mg, 14%. UV/vis spectrum in chloroform [λ_{max}, nm (ϵ, M^{-1} cm^{-1})]: 308 (12000), 430 (16300), 796 (3800), 868 (5700). 300 MHz ^{1}H NMR (chloroform-*d*): δ 6.41 and 5.90 (s, 1 H each, 5,10 *H*), 3.10−2.2 (m, 16 H, CH_2), 1.30−1.05 (m, 24 H, CH_3).

Zn^{II}(HOEB-10-(CN)). Green H_3(OEB-10-(CN)) (11.9 mg, 0.021 mmol) was dissolved in 50 mL of chloroform and heated to reflux temperature. Zinc acetate dihydrate (22.7 mg, 0.104 mmol) was dissolved in 20 mL of methanol and added to the chloroform solution. After 30 min the resulting yellow-green solution was taken to dryness under reduced pressure. Removal of zinc acetate was accomplished by the introduction of cold methanol with agitation and subsequent filtration of the product. The resulting olive-green solid was washed with cold methanol. Yield: 7 mg, 55%. UV/vis spectrum in chloroform [λ_{max}, nm (ϵ, M^{-1} cm^{-1})]: 388 (50300), 790 (18600). 300 MHz ^{1}H NMR (pyridine-d_5): δ 12.06 (br s, 1 H, O*H*), 5.85 (s, 2 H, 5,15-*H*), 3.02 (br q, 4 H, CH_2), 2.40 (br q, 12 H, CH_2), 1.36 (t, 6H, CH_3), 1.22 (t, 6H, CH_3), 1.16 (t, 6H, CH_3), 1.03 (t, 6H, CH_3). IR (Fluorolube mull, cm^{-1}): 3150 br w, 2970 m, 2930 m, 2860 m, 2220 w (ν(CN)), 1690 s, 1660 w, 1620 m, 1560 m, 1530 m, 1500 m, 1480 w, 1450 w, 1380 w, 1360 w, 1320 w, 1300 w, 1280 w, 1260 w, 1200 s, 1160 s, 1140 s, 1060 w, 1020 m, 980 m.

[Zn^{II}(OEOP-15-(CN))](O_2CCH_3). Green H_3(OEB-10-(CN)) (62.8 mg, 0.11 mmol) was dissolved in 50 mL of chloroform and heated under reflux. Zinc acetate dihydrate (100 mg, 0.46 mmol) was dissolved in 20 mL of methanol and added to the chloroform solution. After 10 min the reaction mixture was evaporated to dryness to give a green residue that contained Zn^{II}(HOEB-10-(CN)). This residue was dissolved in 10 mL of acetic anhydride and heated under reflux. After 5 min the contents of the flask were evaporated to dryness. The product was purified by column chromatography on silica with chloroform as eluant. Two unidentified bands (green and red) were allowed to pass through the column. Addition of 2−4% methanol in chloroform to the column eluted the desired product as a broad green band. Yield: 23 mg, 30%. UV/vis spectrum in chloroform [λ_{max}, nm (ϵ, M^{-1} cm^{-1})]: 410 (54000), 640 (8000), 688 (48000). 400 MHz ^{1}H NMR (chloroform-*d*): δ 9.24 (s, 2 H, meso protons), 3.87 (m, 4 H, methylene protons), 3.52 (m, 12 H, methylene protons), 1.64 (m, 24 H, methyl protons).

Zn^{II}(OEB-10,19-(CN)$_2$). [Zn^{II}(OEOP-15-(CN))](O_2CCH_3) (20 mg, 0.030 mmol) was dissolved in 10 mL of dichloromethane with stirring to give a green solution. Tetra(*n*-butyl)ammonium cyanide (39 mg, 0.15 mmol) was added to produce an immediate change in color from green to brown. The reaction solution was poured into 50 mL of dichloromethane and then washed with water (3 × 50 mL). The dichloromethane layer was dried with anhydrous sodium sulfate and evaporated to dryness. The product was purified by column chromatography on silica (25 mm × 150 mm) with 10% ethyl acetate in hexanes as eluant. An unidentified green band eluted first, and a second brown band, identified as Zn^{II}(OEB-10,19-(CN)$_2$), was collected and evaporated to dryness. Yield: 4 mg, 21%. UV/vis spectrum in chloroform [λ_{max}, nm (ϵ, M^{-1} cm^{-1})]: 422 (65000), 896 (13100). 400 MHz ^{1}H NMR (chloroform-*d*): δ 6.94 (s, 1 H, meso proton), 5.86 (s, 1 H, meso proton), 2.93 (m, 4 H, methylene protons), 2.50 (m, 12 H, methylene protons), 1.18 (m, 24 H, methyl protons). IR (Fluorolube mull, cm^{-1}): 2960 s, 2930 s, 2900 m, 2206 m (ν(CN)), 1700 m, 1640 m, 1580 s, 1520 s, 1450 s, 1350 m. MALDI mass spectrum: *m*/*z* 651.35 (M^+).

Zn^{II}(OEB-10,15,19-(CN)$_3$). Method 1. A sample of [Zn^{II}(OEOP-15-(CN))](O_2CCH_3) (27 mg, 0.040 mmol) was dissolved in 25 mL of chloroform with stirring to give a green solution. Tetra(*n*-butyl)-ammonium cyanide (25 mg, 0.093 mmol) was added to the green solution, which was stirred for 2 h. The reaction solution was then poured into 75 mL of chloroform and extracted with water (3 × 100 mL). The chloroform layer was dried with sodium sulfate and evaporated to dryness. The resulting brown oil was purified by column chromatography on silica (25 mm × 150) with 10% acetic anhydride in hexanes as eluant. The first unidentified green band was set aside. The second band (brown), identified as Zn^{II}(OEB-10,15,19-(CN)$_3$), was collected and taken to dryness. Yield: 8 mg, 29%. UV/vis spectrum in chloroform [λ_{max}, nm (ϵ, M^{-1} cm^{-1})]: 444 (13700), 906 (3480). 400 MHz ^{1}H NMR ($CDCl_3$): δ 6.12 (s, 1 H, meso proton), 2.90 (m, 4 H, methylene protons), 2.50 (m, 12 H, methylene protons), 1.15 (m, 24 H, methyl protons). IR (Fluorolube mull, cm^{-1}): 2970 s, 2930 s, 2880 m, 2850 m, 2210 w (ν(CN)), 1720 w, 1670 w, 1550 s, 1500 m, 1460 m, 1380 m. MALDI mass spectrum: *m*/*z* 676.24 (M^+).

Table 4. Crystal Data and Data Collection Parameters

	μ-H_2O-{Zn^{II}(OEB-10,19-$(CN)_3$)}$_2$·0.5acetone·0.6H_2O	μ-H_2O-{Zn^{II}(OEB-10,15,19-$(CN)_3$)}$_2$·acetone	Co^{II}(OEB-15,19-$(CN)_2$)·acetone
formula	$C_{75.80}H_{89.65}N_{12.30}O_{4.10}Zn_2$	$C_{79}H_{90}N_{14}O_4Zn_2$	$C_{40}H_{48}N_6O_2Co$
fw	1369.39	1430.40	703.77
color and habit	black parallelpiped	black plates	black plates
cryst syst	orthorhombic	monoclinic	triclinic
space group	*Pbcn*	*C*2/*c*	$P\bar{1}$
a, Å	23.102(4)	23.3553(11)	11.465(3)
b, Å	15.6338(16)	15.1570(7)	12.133(4)
c, Å	20.557(3)	20.8893(10)	13.833(13)
α, deg	90	90	96.780(4)
β, deg	90	97.4790(10)	96.299(4)
γ, deg	90	90	104.384(4)
V, Å^3	7424.8(17)	7340.5(6)	1831.5(8)
T, K	133(2)	91(2)	90(2)
Z	4	4	2
d_{calcd}, g cm^{-3}	1.225	1.294	1.276
radiation (*λ*, Å)	Cu Kα (1.54178)	Mo Kα (0.71073)	Mo Kα (0.71073)
μ, mm^{-1}	1.230	0.713	0.511
range of transm factors	0.60−0.91	0.78−0.90	0.78−0.96
no. of unique data	4893	11801	6631
no. of params refined	449	479	453
R1[a]	0.080	0.043	0.052
wR2[b]	0.245	0.117	0.143

[a] For data with $I > 2\sigma(I)$. [b] For all data.

Zn^{II}(OEB-10,15,19-$(CN)_3$). Method 2. [Zn^{II}(OEOP-15-(CN))](O_2-CCH_3) (27 mg, 0.040 mmol) was dissolved in 25 mL of chloroform and stirred to give a green solution. Tetra(*n*-butyl)ammonium cyanide (25 mg, 0.093 mmol) was added to the green solution, which was stirred for 2 h. The reaction contents were then poured into 75 mL of chloroform and extracted with water (3 × 100 mL). The chloroform layer was dried with sodium sulfate and taken to dryness. The resulting brown oil was purified by column chromatography on silica (25 mm × 150) with 10% ethyl acetate in hexanes as eluant. The first unidentified green band was set aside. The second band (brown), identified as Zn^{II}(OEB-10,15,19-$(CN)_3$), was collected and taken to dryness. Yield: 8 mg, 29%. Spectral data matches that of the Zn^{II}-(OEB-10,15,19-$(CN)_3$) sample prepared above.

Co^{II}(OEB-15,19-$(CN)_2$). Approximately 10 mg of H_2(OEB-15,19-$(CN)_2$) was dissolved in 5 mL of acetone and titrated with a saturated solution of cobalt(II) acetate in methanol. The insertion reaction was monitored by UV/vis spectroscopy until a complete change from the free-ligand absorbances (412 nm, 778 nm) to the metal-inserted absorbances (440 nm, 796 nm) occurred. Once the metal insertion was complete, the acetone solution was quickly evaporated to dryness. The resulting brown film was redissolved in 1 mL of acetone and transferred to a pipet, which contained a small plug of silica. The acetone effluent, which contained Co^{II}(OEB-15,19-$(CN)_2$), was carefully layered over water in a 5 mm o.d. glass tube. Dark black plates of the product appeared after 3−5 days.

X-ray Data Collection for μ-H_2O-{(Zn^{II}(OEB-10,15,19-$(CN)_3$)}$_2$·acetone and Co^{II}(OEB-15,19-$(CN)_2$)·acetone. Crystals were obtained by layering an acetone solution of Zn^{II}(OEB-10,15,19-$(CN)_3$) over a layer of water in a 5 mm glass tube. Slow diffusion of water into the acetone solution of the complex produced black parallelepipeds. A parallelepiped was coated with a light hydrocarbon oil and mounted in the 91 K dinitrogen stream of a Bruker SMART 1000 diffractometer equipped with a CRYO Industries low-temperature apparatus. Intensity data were collected using graphite-monochromated Mo Kα radiation. Crystal data are given in Table 4.

X-ray Data Collection for μ-H_2O-{Zn^{II}(OEB-10,19-$(CN)_2$)}$_2$·0.5acetone·0.6H_2O. Crystals were obtained by layering an acetone solution of Zn^{II}(OEB-10,19-$(CN)_2$) over a layer of water in a 5 mm glass tube. Slow diffusion of water into the acetone solution of the complex produced black parallelepipeds. A parallelepiped was coated with a light hydrocarbon oil and mounted in the 133 K dinitrogen stream of a Siemens P4 diffractometer equipped with a Siemens LT-2 low-temperature apparatus. Intensity data were collected using graphite-monochromated Cu Kα radiation. Crystal data are given in Table 4. Two check reflections showed only random (<1%) variation in intensity during data collection. The data were corrected for Lorentz and polarization effects.

Solution and Structure Refinement. Calculations were performed with the SHELXTL 5 series of programs. Scattering factors and correction for anomalous dispersion were taken from a standard source.[34] An absorption correction was applied to μ-H_2O-{Zn^{II}(OEB-10,19-$(CN)_2$)}$_2$·0.5acetone·0.6H_2O[35a] and to Co^{II}(OEB-15,19-$(CN)_2$)·acetone.[35b] The solutions were determined by direct methods and subsequent cycles of least-squares refinement and calculation of difference Fourier maps.

Calculation Methods. Local density functional calculations were performed using the SVWN implementation of the Vosko−Wilk−Nusair (VWN) local exchange-correlation potential in Spartan 5.0,[36] DN** basis sets, and a fine mesh for numerical integrations. Starting geometries were obtained from Spartan's graphical builder. Symmetry constraints generally were not imposed on the geometry optimizations.

Acknowledgment. We thank the NIH (GM-26226) for support. A.M.S. thanks the University of West Virginia for granting a sabbatical leave.

Supporting Information Available: X-ray crystallographic files in CIF format for μ-H_2O-{Zn^{II}(OEB-10,19-$(CN)_2$)}$_2$·0.5acetone·0.6H_2O, μ-H_2O-{(Zn^{II}(OEB-10,15,19-$(CN)_3$)}$_2$·acetone, and Co^{II}(OEB-15,19-$(CN)_2$)·acetone. This material is available free of charge via the Internet at http://pubs.acs.org.

IC0103300

(34) *International Tables for Crystallography*; Kluwer Academic Publishers: Dordrecht, The Netherlands, 1992.
(35) (a) XABS: Parkin, S.; Moezzi, B.; Hope, H. *J. Appl. Crystallogr.* **1995**, *28*, 53. (b) SADABS 2.0, Sheldrick, G. M., 2000.
(36) Spartan version 5.0, Wavefunction Inc., 18401 Von Karman Ave., Suite 370, Irvine, CA 92612.